

1 **Determining finite strain: how far have we progressed?**

2 Dave McCarthy<sup>1</sup>, Patrick Meere<sup>2</sup> and Kieran Mulchrone<sup>3</sup>

3 1 British Geological Survey, The Lyell Centre, Research Avenue South, Edinburgh, EH14 4AP, UK

4 2 School of Biological, Earth and Environmental Sciences, University College, Cork, Ireland

5 3 Department of Applied Mathematics, University College, Cork, Ireland

6 **Abstract**

7 One of the main aims in the field of structural geology is the identification and quantification of  
8 deformation or strain. This pursuit has occupied geologists since the 1800's, but has evolved  
9 dramatically since those early studies. The quantification of strain in sedimentary lithologies was  
10 initially restricted to lithologies of known initial shape, such as fossils or reduction spots. In 1967,  
11 Ramsay presented a series of methods and calculations, which allowed populations of clasts to be  
12 used as strain markers. These methods acted as a foundation for modern strain analysis, and have  
13 influenced thousands of studies. This review highlights the significance of Ramsay's contribution to  
14 modern strain analysis. We outline the advances in the field over the 50 years since publication of the  
15 'Folding and Fracturing of Rocks', review the existing limitations of strain analysis methods and look  
16 to future developments.

17

18 *'The analysis of the variation in amount of finite strain in a deformed zone is of the utmost importance*  
19 *in helping to understand the structural geometry and hence the structural history of the rocks.'*

20

*John Ramsay, 1967*

21 The field of structural geology is primarily concerned with understanding the deformation of crustal  
22 rocks. This deformation or strain is caused when external forces or stresses act on a rock mass, causing  
23 a change in its shape or size (Ramsay, 1967). The concept of quantifying strain in rocks has been  
24 prevalent since the 1800's, and has evolved dramatically since those early studies. Various methods  
25 have been used to identify and quantify strain, the earliest of which relied on objects of a known initial

26 shape. This approach was first taken by Phillips (1843) and Sharpe (1847) who used deformed fossils,  
27 with Sharpe (1847) noting that the most deformed fossils were present in the areas with the most  
28 intense cleavage. This led to Sorby's seminal interpretations of cleavage development (Sorby, 1849)  
29 and correlation of cleavage to areas with high strain (Sorby, 1856). Haughton (1856) provided the first  
30 mathematical description of length changes in fossils due to strain in naturally deformed rocks,  
31 furthermore, he applied the concept of the strain ellipsoid to rock deformation, which established a  
32 framework for strain to be quantified and compared.

33 It was not until the quantitative studies on distorted ooids by Cloos (1947) that truly numerical and  
34 methodological strategies were fully applied to strain analysis. By the early 1960's, strain analysis  
35 methods were still largely dependent on the presence of strain markers of known initial shape, such  
36 as fossils, ooids or reduction spots (Breddin, 1954, 1957; DeSitter, 1964). In 1967, John Ramsay  
37 presented a suite of precise and mathematical procedures that allowed for the accurate  
38 determination of finite strain in deformed rocks. These methods, though significantly modified, have  
39 stood the test of time and are regularly employed. Of the many publications citing Ramsay's *Folding*  
40 and *Fracturing*, a significant number, >1000, have focussed on strain analysis (Lisle, this issue). It is  
41 clear that these techniques are still applied to both field studies and mathematical models of rock  
42 deformation.

43 This review starts by highlighting the importance of Ramsay's initial contribution, then we outline the  
44 significant advances in the techniques of strain analysis made over the last 50 years. This is followed  
45 with a brief discussion on applications of strain analysis and how these techniques have advanced our  
46 understanding of natural rock deformation. There is clearly a huge body of research involving strain  
47 analysis and it is not possible to reference every application here, but we have highlighted some key  
48 developments. We then follow this by providing a discussion of some of the key unresolved problems  
49 in the field. We conclude with some ideas for future directions and hope that this will act as a  
50 springboard for those investigating strain in rocks for the first time.

51 **Strain Analysis Techniques proposed by Ramsay**

52 The significance of Ramsay's contribution was that he set out in a systematic and mathematical  
53 manner techniques for determining strain from objects of known initial shape, and he established  
54 methods which allowed populations of objects, such as sedimentary clasts, of non-spherical and  
55 fluctuating initial shape, to be used as strain markers. These methods depend on clast orientation,  
56 repacking and intraclast deformation of clasts due to deformation. This was a key development in  
57 strain analysis, as it allowed estimates to be made from lithologies that did not have obvious or  
58 established strain markers (Fig. 1). The methods developed by Ramsay (1967) are briefly outlined  
59 below:

60 *Method 1*

61 The first method that Ramsay outlined built on existing techniques at the time, and involved direct  
62 measurement of the principal axes of elliptical strain markers and the orientation of their long axes  
63 (Ramsay, 1967, p 193). These axes are then plotted against each other (Fig. 2a) and the slope of the  
64 best-fit line that also passes through the origin provides an estimate of the strain ratio (Fig. 2b).  
65 Ramsay noted it was difficult to accurately identify ellipse lengths in high deformation regimes, and  
66 that it was difficult to identify the maximum stretching direction in low strain regimes.

67 *Method 2*

68 The second method (Ramsay, 1967, p 193-194), does not rely on direct measurement of ellipse axes,  
69 and accounts for difficulties in methods of identifying the length of maximum ellipse axes. The centre  
70 of each ellipse is identified and the lengths of chords from the centre to the edge of each ellipse along  
71 three arbitrarily directions are measured. The sum of the chord lengths for the three defined  
72 directions for a population of objects is calculated (Fig. 2c). If the objects were initially circular, the  
73 ratios of elongation can be calculated for each direction.

74

75            *Method 3*

76    This method, commonly referred to as the nearest-neighbour or centre-to-centre method, (Ramsay,  
77    1967, p 195-196) was developed to tackle cases where pressure solution was suspected to have  
78    occurred, and is applicable to rocks with particles equally or unequally distributed throughout the rock  
79    mass. In cases where pressure solution is a significant deformation mechanism, the elliptical shape or  
80    preferred orientation of markers is not reliable. This method is particularly useful for identifying cases  
81    where non-passive deformation is thought to have occurred (i.e. that the clasts are not deforming  
82    homogeneously with the matrix). The basic premise involves measuring the distance between object  
83    centres, and assuming that in the unstrained state these distances should be isotropic (Fig. 3a). During  
84    deformation the distance between centres should become shorter parallel to the maximum  
85    compression axis (Fig. 3b & c).

86            *Method 4*

87    The fourth method (Ramsay, 1967, p 197-199) utilised the measurements of distorted angles of radial  
88    and tangential lines in elliptical sections, such as those in spherulites. Whilst an elegant method of  
89    calculating strain, this method has had limited use due to the specific nature of the strain markers  
90    required.

91            *R<sub>f</sub>/∅ Method*

92    In addition to the four methods above, Ramsay (1967, p 204-211) also outlined a method for  
93    specifically dealing with markers of initial elliptical, the R<sub>f</sub>/∅ method (Fig. 4), where R<sub>f</sub> is the deformed  
94    axial ratio of the marker ellipsoid, while ∅ is the orientation of the long axis. This is slightly more  
95    complex than using initially circular objects, in that when an ellipse is deformed under homogeneous  
96    conditions, the resulting shape is another ellipse. The axial ratio (R<sub>f</sub>) and orientation of the deformed  
97    ellipse is a result of the combination of the initial aspect ratio (R<sub>i</sub>) and orientation (θ), and the strain

98 ellipse, all of which are unknowns. When a population of deformed ellipses are considered, variations  
99 in their  $\emptyset$  values can be related to eccentricity in their orientations prior to deformation.

#### 100 **Measuring strain after Ramsay**

101 Essentially Ramsay (1967) developed methods whereby strain estimates could be made using  
102 parameters derived from the following: strain marker orientation, strain marker shape, position of  
103 strain marker centres, distance between centres and the angle between centres. The two main types  
104 of methods that prevailed were the  $R_f/\emptyset$  method and the centre-to-centre. The  $R_f/\emptyset$  method (Fig. 4)  
105 determines finite strain from randomly oriented populations of deformed elliptical objects, while the  
106 centre-to-centre method (Fig. 3) uses the distance between centres of adjacent objects, and assumes  
107 the objects were uniformly distributed prior to deformation.

108 Subsequent to the initial  $R_f/\emptyset$  method, alternative methods based on marker shape and orientation  
109 were developed (Dunnet, 1969; Elliott, 1970; Dunnet and Siddans, 1971; Matthews et al., 1974;  
110 Borradaile, 1976; Shimamoto and Ikeda, 1976; Lisle, 1977a, 1977b, 1985; Robin, 1977; Peach and Lisle,  
111 1979; Siddans, 1980; Yu and Zheng, 1984; Mulchrone and Meere, 2001; Mulchrone et al., 2003).  
112 Dunnet (1969) developed an  $R_f/\emptyset$  diagram method, while Elliott (1970) applied a similar graphical  
113 approach, the shape factor grid. Dunnet and Siddans (1971) took non-random initial orientations into  
114 consideration for the  $R_f/\emptyset$  diagram method. A significant drawback of these methods is that they are  
115 subjective.

116 An algebraic method that accommodated statistical analysis of any errors produced was introduced  
117 by Matthews et al. (1974). The drawback of this method was that the orientation of the principal strain  
118 axis needed to be calculated independently prior to using the method. Similarly, Robin (1977) derived  
119 a method that allowed analysis of strain markers of any shape but required prior independent  
120 knowledge of the principal strain axes. Advances in the  $R_f/\emptyset$  method are discussed in further detail by  
121 Lisle (1994). In order to address the issues outlined above with calculating strain from distributions of  
122 elliptical objects, Shimamoto and Ikeda (1976) developed an objective non-graphical, reproducible

123 approach to strain analysis. This approach averaged the parameters of all of the marker ellipses to  
124 generate one marker ellipse, or if the initial distribution was isotropic, a marker circle. The Mean Radial  
125 Length (MRL) method of Mulchrone et al. (2003) took a similar approach, whereby the average shape  
126 of a population of isotropic ellipses or non-deformed sedimentary clasts equates to a circle. As this  
127 population becomes deformed by either shape change or rotation, this circle becomes an ellipse  
128 and can be directly related to the strain ellipse in the same manner that any circular marker can  
129 after deformation.

130 The centre-to-centre family of techniques are based on using object-to-object separation and assume  
131 that the distribution of marker objects are isotropic and that after deformation the distance between  
132 any marker centre and all other clast centres has been modified. The relative change in clast centres  
133 distances can be related to the direction and magnitude of the finite strain ellipse (Ramsay, 1967).  
134 Compared to the  $R_f/\phi$  method, the centre-to-centre method involved relatively complicated  
135 calculations and was particularly labour intensive. As a result, it initially received significantly less  
136 attention than the  $R_f/\phi$  method. This changed when a relatively simple graphical approach was  
137 developed by Fry (1979; Hanna and Fry, 1979), which used all object-object separations. This was  
138 subsequently further improved as the Normalised Fry Method (Erslev, 1988) and the enhanced  
139 Normalised Fry Method (Erslev and Ge, 1990). McNaught (1994) further extended these methods by  
140 facilitating the use of non-elliptical markers by determining best-fit ellipses for these irregular shaped  
141 objects. One of the drawbacks of the centre-to-centre techniques is that they do not account for  
142 volume loss, which can be considerable when pressure solution is a dominant deformation mechanism  
143 (Onasch, 1986; Dunne et al., 1990). Furthermore, if pressure solution is significant, there are  
144 difficulties in identifying the pre-strain centres of clasts and if significant heterogeneous deformation  
145 is present at the clast scale than this can lead to further underestimates of strain.

146 The Fry methods have been regularly incorporated into automated analysis tools (Ailleres et al., 1995;  
147 Launeau and Robin, 1996; Launeau et al., 2010). Despite popularity and ease of use, these methods

148 are subjective, with interpreter bias being introduced at both the identification of clast centres, and  
149 the definition of the central ellipse on the Fry plot. Mulchrone (2003) used Delaunay triangulation to  
150 characterise nearest neighbour separations, and defined object centres using the centroid of the best-  
151 fit ellipse. This resulted in a more objective and automated process for identifying object centres and  
152 creating the tie-lines between nearest neighbours.

### 153 *Calculating the strain ellipsoid*

154 Most strain analysis techniques focus on quantifying strain in a 2D plane. In order to quantify strain in  
155 3D, a strain ellipsoid needs to be defined. Typically, the strain ellipsoid is defined from strain ellipses  
156 on several planar surfaces with differing orientations. Similar to calculating the strain ellipse,  
157 calculating the strain ellipsoid is not a trivial process, and numerous attempts have been made at  
158 determining the most accurate best-fit ellipsoid. Ramsay (1967; p. 142-147) derived a series of  
159 equations to solve for the best-fit ellipsoid from three mutually perpendicular planes. Numerical  
160 algorithms were subsequently developed for three orthogonal sections (Shimamoto and Ikeda, 1976;  
161 Oertel, 1978). This was followed by methods, which allowed for non-orthogonal sections (Milton,  
162 1980; Gendzwill and Stauffer, 1981; Shao and Wang, 1984; De Paor; 1990). Owens (1984) in particular  
163 described an iterative method for the calculation of the best-fit strain ellipsoid from any number of  
164 non-perpendicular sections using a least squares approach, as well as applying a scale factor. Robin  
165 introduced an approach utilising a series of linear equations (Robin, 2002; Launeau and Robin, 2005).  
166 Shan (2008) built on the Robin method, and included added flexibility, whereby stretching lineation  
167 data could be included. The important distinction of the Robin and Shan methods from the previous  
168 methods was that they were non-iterative but separated the parameters to be calculated from the  
169 initial data. Vollmer (2017) has provided a more detailed comparison of the Robin and Shan methods,  
170 as well as applying bootstrap statistics to the results. Mookerjee and Nickleach (2011) presented a  
171 suite of methods in Mathematica, which attempts to minimise the errors between the best-fit ellipsoid  
172 and any of the measured planes used as input data.

174 The geometries of strain ellipsoids can be represented in 2D space using a Flinn Plot (Flinn, 1956, 1962,  
175 1965). This type of plot was first used to compare the elliptical properties of clast populations in  
176 conglomerates (Zingg, 1935). The ratio of the maximum to intermediate ellipsoid axes ( $R X/Y$ ) is  
177 plotted as ordinate and the ratio of the minimum to intermediate axes ( $R Y/Z$ ) is plotted as abscissa  
178 on these graphs. The Flinn Plot was subsequently modified by Ramsay (1967) to include a logarithmic  
179 scale (Fig. 5; discussed further in Hobbs et al., 1976; Ramsay and Huber, 1983). The benefit of the  
180 logarithmic Flinn Plot is that it provides a more even distribution of points with increase in deformation  
181 (Ramsay and Huber, 1983), whilst in the original Flinn Plot low strains are clustered near the origin,  
182 making it difficult to interpret data.

183 The symmetry of the strain ellipsoid can be described by the ratio  $K ((X/Y)/(Y/Z))$ . If  $K > 1$  then the  
184 ellipsoid is considered to have a prolate or axial symmetric constriction and has one long axis and two  
185 shorter axes. If  $K < 1$  the ellipsoid is considered to be oblate or axially symmetrically flattened and has  
186 two long axes and one shorter axis. Between these two fields of flattening and constriction is the field  
187 of plane strain ( $K=1$ ) and which only occurs when strain is acting in the XZ plane.  $K$  represents the slope  
188 of a line from the data point to the origin at (1,1), so that  $K = a-1/b-1$  with  $a=x/y$  and  $b=y/z$ .  $K$  on the  
189 diagram can define a series of domains, so that when  $K=0$  the finite strain ellipsoid is uniaxial oblate  
190 and has been flattened perpendicular to  $Z$ . As  $K$  tends towards 1 the ellipsoid moves away from being  
191 purely uniaxial, but remains in the oblate and flattened domain. For  $K$  values greater than 1 the  
192 ellipsoid lies in the prolate or constrictive domain, and for  $K=\infty$  the ellipsoid is purely uniaxial prolate  
193 and stretched along the  $X$  axis (Park, 1997). The degree of how far removed the ellipsoid is from  
194 spherical (ellipsoid eccentricity) is calculated as  $\sqrt{((X/Y)^2 + (Y/Z)^2)}$ .

195 A less-popular alternative to the Flinn Plot, the Nadai-Hsu Plot (Fig. 5; Nadai, 1950; Hsu, 1966) was  
196 first applied to geological strain analysis by Hossack (1968). This type of plot presents strain in a polar  
197 area, and is argued to provide a less distorted representation of the deviatoric strains (Hobbs et al.,

198 1976; Brandon, 1995; Mookerjee and Peek, 2014). Another advantage of this type of polar plot is that  
199 ellipsoids with low strain ratios plot closer together regardless of the ellipsoid shape. Ramsay and  
200 Huber (1983) criticised the Nadai-Hsu plots, irrotational strain is assumed, while most natural  
201 deformation involves progressive non-coaxial rotational strains.

202 The fundamental difference is that the Nadai-Hsu Plots use the *amount of strain* ( $\epsilon_s$ ) and Lode's Ratio  
203 ( $v$ ), to define the ellipsoid shape (Lode, 1926). The *amount of strain*, is related to the octahedral shear,  
204  $Y_o$ , and is defined by:  $\epsilon_s = (\sqrt{3} / 2) Y_o$ , where  $Y_o = (2/3) [(\epsilon_1 - \epsilon_2)^2 + (\epsilon_2 - \epsilon_3)^2 + (\epsilon_3 - \epsilon_1)^2]^{1/2}$  and  $\epsilon_1$ ,  
205  $\epsilon_2$  and  $\epsilon_3$  represent the strain axes. The Lode Ratio is defined as  $v = (2\epsilon_2 - \epsilon_1 - \epsilon_3) / (\epsilon_1 - \epsilon_3)$  and  
206 ranges from -1 to 1. Lode ratios of -1 define a prolate ellipsoid, while 1 and 0, define an oblate and  
207 plane strain ellipsoid respectively. Whereas the Flinn Plot solely relies on the aspect ratios of the strain  
208 ellipsoid (as discussed above). For a more in depth discussion of the merits of each method readers  
209 are referred to Mookerjee and Peek (2014) and Vollmer (2017).

#### 210 *Automation*

211 Possibly one of the biggest drawbacks to most strain analysis studies is the high labour intensity  
212 required for both the identification of object boundaries, and the accurate identification of their  
213 centres for enough objects to create a statistically robust sample set. Since the late seventies, many  
214 attempts have been made at automating strain or fabric analysis to address this (e.g., Peach and Lisle,  
215 1979). Initially, the limiting steps in the automation of these strain analysis techniques was the  
216 recognition and fitting of best-fit ellipses to geological strain markers, such as sedimentary clasts (Fig.  
217 6a & b).

218 The efficient and accurate automatic segmentation of thin section images is still a developing field and  
219 has received a lot of recent attention with numerous attempts at automated extraction using image  
220 processing or GIS-based techniques (e.g., Goodchild and Fueten, 1998; Heilbronner, 2000; van den  
221 Berg et al., 2002; Perring et al., 2004; Barraud, 2006; Choudhury et al., 2006; Li et al., 2008; Tarquini  
222 and Favalli, 2010; DeVasto et al., 2012; Gorsevski et al., 2012; Heilbronner and Barrett 2013;

223 Mingireanov Filho et al., 2013; Jungmann et al., 2014; Asmussen et al., 2015). Although these methods  
224 produce rapid grain boundary maps, they are typically inaccurate or achieve different results  
225 depending on the nature of the image. This is highlighted by the regular use of quartz clasts as strain  
226 markers, whereby the automatic identification of their boundaries is complicated by undulose  
227 extinction, deformation bands, diffuse boundaries and colour similarities between neighbouring  
228 grains. Despite these advances, most methods follow the approach of Mukul (1998), whereby grains  
229 used as strain markers are manually traced, and then analysed using image analysis software.

230 A number of methods for automated image analysis have been successfully utilised in the past for  
231 geological strain analysis (Ailleres et al., 1995; Erslev and Ge, 1990; Masuda et al., 1991; McNaught,  
232 1994; Heilbronner and Barrett, 2013). Panozzo (1984) utilised digitised sets of points representing  
233 linear or elliptical objects in her projection method. Mulchrone et al. (2005) developed a parameter  
234 extraction program (SAPE) that rapidly extracts the required data by using a simple region-growing  
235 algorithm to identify regions of interest. Vollmer developed a similar method, Ellipsefit (Vollmer, 2010,  
236 2011, 2017). Many of these techniques are discussed in Heilbronner and Barrett (2013), who have  
237 provided a superb overview of image analysis techniques for geological material and it is  
238 recommended as a starting point for readers interested in this field.

239 Once grain boundaries have been identified and ellipses are fitted to clasts, the parameters required  
240 for a range of strain analysis techniques such as the aspect ratio, orientation, and the centroid of the  
241 object can now be easily extracted. For the  $R_f/\phi$  method the difficulties in calculating a strain estimate  
242 cease once ellipses have been fitted to strain markers; for the centre-to-centre methods the  
243 difficulties continue.

244 The accuracy of centre-to-centre strain estimates can be further hampered by the ability to clearly  
245 define the vacancy field or central void of the Fry Plot (Fig. 6c), which in a strained sample should  
246 represent the strain ellipse (Crespi, 1986; Waldron and Wallace, 2007). A variety of techniques have  
247 been applied in order to accurately and objectively define this void (Erslev and Ge, 1990; McNaught,

248 1994; Waldron and Wallace, 2007; Lisle, 2010; Shan and Xiao, 2011; Reddy and Srivastava, 2012;  
249 Mulchrone, 2013). Similar problems exist for defining the curve of the polar plot (Mulchrone, 2013).

250 In order to reduce the time and labour intensity required, Mulchrone et al. (2013) integrated image  
251 analysis, ellipse fitting and parameter extraction, and strain analysis routines for MRL and DTNNM in  
252 one workflow. They also included a method for bootstrapping the results in order to produce  
253 uncertainty estimates (Fig. 6 e&f). Kumar et al. (2014) carried out a detailed comparison analyses on  
254 these methods, and found that the Delaunay Triangulation Method of Mulchrone (2013) and the  
255 Continuous Function Method of Waldron and Wallace (2007) were the most accurate. Additionally  
256 they concluded that the Delaunay Triangulation Method and the image analysis technique of Reddy  
257 and Srivastava (2012) were the most time efficient.

258 The other method that has stood out is the SURFOR method, first presented by Panozzo (1984, 1987),  
259 and discussed in detail in Heilbronner and Barrett (2013). The SURFOR method takes a slightly  
260 different approach to fabric or strain analysis compared to the Ramsay family of methods. Rather than  
261 focussing on the object orientation or the spatial relationship between objects, the SURFOR method  
262 quantifies the fabric based on the shape, size and orientation of 'surfaces' (Heilbronner and Barrett,  
263 2013). The 'surfaces' can be any linear element, such as fractures or grain boundaries. One particular  
264 advantage of the SURFOR method over the original Ramsay  $Rf/\phi$  method is that it accounts for marker  
265 size, with smaller objects having less of an impact on the final strain/anisotropy estimate. A similar  
266 approach is taken by Launeau et al. (1990, 1996, 2010), whereby linear filters are used to count  
267 intercepts along any arbitrary direction of a digital image. The intercepts technique has shown to be  
268 comparable to the MRL and the DTNNM methods in moderate strain regimes, although in low strain  
269 regimes there appears to be a discrepancy between the methods (McCarthy et al., 2015). These  
270 discrepancies are due to uncertainties in strain estimates in low strain regimes.

271

272 **Application of strain analysis and advances in strain theory**

273 This contribution has focussed on the significant advances made in geological strain analysis, as  
274 outlined above, which have provided a number of valuable insights into geological deformation.  
275 Unfortunately, natural deformation is rarely simple or restricted to 2D planes, yet this approach have  
276 aided with understanding of complex deformations.

277 Strain analysis and resulting knowledge of the finite strain state of a point in a rock mass has played a  
278 fundamental part in the understanding of the development of tectonic fabrics and foliations (Ramsay  
279 and Wood, 1973, Tullis and Wood, 1975). However, nature tends to reveal more by capturing change  
280 in strain through time and space, (e.g. porphyroclasts and related structures, layers which are  
281 shortened and then stretched, and regions of intense shear where the continuum from low to high  
282 strain can be spatially traced). Often the spatial changes can be interpreted as reflecting the temporal  
283 deformation history. Ramsay (1967) applied the concept of infinitesimal strain together with that of  
284 finite strain to understand deformation history, with the difference between what happens in a short  
285 time step compared to that over long time periods helped develop the ideas of progressive strain. This  
286 infinitesimal approach was followed by the seminal work of Means et al. (1980) who considered the  
287 velocity gradient tensor to conceptualise progressive deformation, and used vorticity to quantify  
288 rotational deformation. A detailed discussion of vorticity is beyond the scope of this contribution, and  
289 interested readers should consult the work of Fossen and Tikoff (Fossen and Tikoff, 1993; Tikoff and  
290 Fossen, 1993; Tikoff and Fossen, 1995; Tikoff and Fossen, 1999; Passchier and Trouw, 2005).

291 Many of the 2D finite strain methods discussed in previous sections have a natural extension to 3D,  
292 but there is still a dearth of 3D strain studies. Methods based on shape (e.g. Shimamoto and Ikeda,  
293 1976; Mulchrone et al., 2003) and inter-object relationships (e.g. Fry, 1979; Mulchrone, 2013) can be  
294 readily developed into 3D methods. However, in many cases the primary difficulty rests with acquiring  
295 suitable data in 3D in order to apply the methods. Recent technological advances have seen the  
296 application of tomography to the acquisition of high quality images of 3D markers in rocks (Louis et al,

297 2006; Adam et al, 2013; Robin and Charles, 2015). This is certain to be an area of future development  
298 and will inform finite strain studies and their interpretation in the context of 3D deformation history  
299 (Tikoff and Fossen, 1999).

300 Important comparisons have been made between clast-based strain analyses and other methods of  
301 quantifying deformation. A number of studies in the seventies and eighties highlighted a close  
302 relationship between finite strain estimates and quartz crystallographic fabrics (Marjoribanks, 1976;  
303 Miller and Christie, 1981; Lisle, 1985; Law, 1986). Rapid developments in techniques such as Electron  
304 Back Scatter Diffraction (EBSD) have largely confirmed this relationship, but also provided insights into  
305 deformation at subgrain scales one of the most prominent methods for the determination of preferred  
306 orientation of minerals in thin sections (Passchier and Trouw, 2005; Prior et al., 2009).

307 Similar advances in rock deformation studies have been made in the field of Anisotropy of Magnetic  
308 Susceptibility (AMS), with Graham (1954) first suggesting that magnetic fabrics could be a valuable  
309 tool in petrofabric analysis and establishing a link between layer parallel shortening and AMS. Since  
310 this pioneering study there has been a huge volume of work confirming the ability of AMS to  
311 determine the orientation-distribution of all minerals and all subfabrics in a specimen, with  
312 comprehensive reviews provided by Borradaile and Henry (1997) and Borradaile and Jackson (2010).  
313 In direct comparisons of AMS to strain analysis techniques, AMS has been shown to be a highly  
314 sensitive and rapid method for quantifying tectonic fabrics (Burmeister et al., 2009; Weil and Yonkee,  
315 2009; McCarthy et al., 2015).

316 Other significant contributions of strain analysis includes providing accurate information for structural  
317 restorations. Compaction and stratigraphic thickening due to deformation can be estimated and  
318 incorporated in the construction of balanced cross sections (Woodward et al., 1986; Protzman and  
319 Mitra, 1990; Mitra, 1994). Despite Layer Parallel Shortening (LPS) or internal deformation  
320 (compaction, collapse of pore space, dissolution or cleavage formation) being shown to accommodate  
321 significant shortening in balanced cross sections from carbonate duplexes (27%; Cooper et al., 1983),

322 gravity driven thrust systems (18-25%; Butler and Paton, 2010), and analogue models (15-30%; Koyi  
323 et al., 2004; Burberry, 2015; Lathrop and Burberry, 2017), strain analysis techniques are rarely applied  
324 to balancing cross sections.

### 325 **Unresolved issues in strain analysis**

326 Hobbs and Talbot (1966) highlighted a few of the limitations of strain analysis a year before Ramsay  
327 published his seminal text, and the majority of these seem to prevail today: the initial shapes of many  
328 strain markers cannot be measured accurately enough to yield highly accurate estimates; and  
329 homogeneous strain is typically assumed. Although these assumptions still prevail, they have largely  
330 been accepted to be unresolved. In addition to this, a number of factors add further uncertainty to  
331 any strain estimate including: strength and influence of the primary or pre-strain fabric; effects of non-  
332 passive strain; and the effects of volume-change, these are discussed below.

#### 333 *Primary fabrics*

334 The largest problem for strain analysis methods is the uncertainty regarding the strength and  
335 orientation of an initial primary fabric. Most strain analysis methods, particularly the  $R_f/\phi$  family of  
336 techniques, rely on the assumption that the strain markers have a random initial orientation. Certainly  
337 in the case of sedimentary rocks this is rarely true, as most sediments develop a preferred orientation  
338 either due to depositional processes or diagenesis (Elliott, 1970; Dunnet and Siddans, 1971; Boulter,  
339 1976; Seymour and Boulter, 1979; De Paor, 1980; Holst, 1982; Paterson and Yu, 1994; Maffione and  
340 Morris, 2017).

341 In a study of undeformed lithologies Holst (1982) found that sections not parallel with bedding had a  
342 preferred orientation of clasts along the trace of the bedding plane, while sections parallel to bedding  
343 typically had no preferred orientation of clasts. Even if an isotropic or random depositional fabric  
344 existed, a preferred orientation typically develops during diagenesis and compaction through active  
345 or partly rigid body rotation (Borradaile, 1987). Several efforts have been made to remove the effects

346 of primary fabrics on strain estimates (Elliott, 1970; Dunnet and Siddans, 1971; Matthews et al., 1974;  
347 Shimamoto and Ikeda, 1976; Lisle, 1977a; Seymour and Boulter, 1979; Holst, 1982; Wheeler, 1986;  
348 DePaor, 1988). Unfortunately, most of these methods utilise one or more of the above assumptions  
349 and/or assume the existence of independent information concerning the strain ellipsoid. Some of  
350 these assumptions regarding the primary fabrics of sedimentary rocks were highlighted by Patterson  
351 and Yu (1994) and include the following: individual grains are spherical prior to straining; orientations  
352 and shapes of grain populations define spherical, pre-strain fabric ellipsoids (i.e. grains have an initial  
353 uniform distribution); pre-strain fabric ellipsoids are symmetric around bedding; and initial fabrics are  
354 recognisable even after straining.

355 Failing to account for any of these factors can lead to considerable errors in strain estimates,  
356 particularly in domains with relatively low strains ( $R < 1.5$ ). To account for these errors Patterson and  
357 Yu (1994) suggested that a correction should be applied by multiplying the estimated strain ellipsoid  
358 by an average pre-strain ellipsoid. Unfortunately, information regarding the magnitude and  
359 orientation of the pre-strain ellipsoid is rarely available. Paterson and Yu (1994) compiled XYZ averages  
360 for a range of rock types, but this is a limited data set and should be expanded. Regarding the  
361 orientation, the estimated strain ellipsoid can be multiplied by the reciprocal pre-strain ellipsoid  
362 multiple times in numerous orientations to create an error bracket. Ramsay (1967) showed that all  
363 possible combinations of two ellipsoids result in an approximate triangular region on a Flinn plot.  
364 Following the methodology of Paterson and Yu (1994), this triangular region is then representative of  
365 the error bars of the strain estimate.

366

### 367 *Non-passive deformation*

368 A key assumption of most current strain analysis techniques is that strain is homogenous and that  
369 markers behave in a wholly passive manner in relation to their host material. This breaks down in most  
370 natural materials especially when sedimentary clasts are used for strain analysis.

371 Clearly, the most ideal strain markers are those that were originally spherical, which were then  
372 deformed passively with no competency contrast between the marker and the host rock. If this holds  
373 true then the final shape of the marker will reflect that of the finite strain ellipsoid (Ramsay, 1967).  
374 The fundamental assumption of most strain analysis methods is that there is no competency or  
375 ductility contrast between the markers and their matrix/host rock, so that the marker and surrounding  
376 rock matrix responded to deformation identically. Unfortunately, clasts and their surrounding matrix  
377 rarely deform in a passive manner, due to competency or ductility contrasts between the marker and  
378 the host rock. This competency contrast is inherently linked to the viscosity contrast between different  
379 clast types and the matrix (Ramsay, 1967; Gay, 1968a,b, 1969; Lisle, 1985b; Freeman, 1987; Freeman  
380 and Lisle, 1987; Treagus, 2002; Mulchrone and Walsh, 2006; Czeck et al., 2009). Gay (1968a) pointed  
381 out that clasts with a low viscosity deform faster than the bulk rock strain ellipse, while clasts with  
382 high viscosities resisted deformation and deformed slower than the bulk rock strain ellipse. Gay  
383 (1968a) also noted that the viscosity ratio between a clast and the matrix is dependent on the relative  
384 proportion of clasts and matrix. Freeman and Lisle (1987) confirmed that the errors in strain estimates  
385 are higher when the clasts represent a small fraction of the bulk rock. This is driven by the high ductility  
386 contrast, whereby the majority of strain is accommodated by the weaker matrix. As the clast-to-matrix  
387 ratio increases the ductility contrast reduces, potentially caused by the reduced ability of the matrix  
388 to flow due to the increase in clast on clast interaction. This separation of strain behaviour between  
389 the matrix and clasts is typically termed strain partitioning. This type of behaviour is largely controlled  
390 by object concentration and the degree of packing and clast interaction, due to the effect these have  
391 on the viscosity contrasts (Gay, 1968a; Lisle et al., 1983; Mandal et al., 2003; Vitale and Mazzoli, 2005).  
392 Generally, lithologies with higher object concentrations display reduced effects of strain partitioning,  
393 leading to more accurate strain estimates (Mandal et al., 2003; Vitale and Mazzoli, 2005).

394 While reviewing problems arising from these competency contrasts, Treagus and Treagus (2002)  
395 concluded that conglomerates as a whole deformed at an approximately constant viscosity in a  
396 linearly viscous manner, but also found that  $R_f/\phi$  style methods characterised clast strain whereas the

397 centre-to-centre methods were more effective at characterising bulk rock strain. This is in part due to  
398 two factors: clasts typically only represent 50-70% of the bulk rock (Leeder, 1982); and the  $R_f/\phi$   
399 methods only consider clast shape and orientation, while centre-to-centre techniques account for  
400 distances between the clasts.

401 This non-passive deformation can be accounted for by utilising centre-to-centre methods, which  
402 include spatial information in the estimates of strain, and provide bulk-rock strain estimates that are  
403 closer to true strain values. This has been illustrated in a range of natural settings (Meere et al., 2008,  
404 Soares and Dias, 2015). Meere et al. (2008) attributed non-passive deformation to the presence of a  
405 relatively incompetent clay-rich matrix, which effectively cushioned clasts from internal deformation.  
406 This type of behaviour allows for high degrees of competent clast long-axis alignment achieved by a  
407 combination of rigid body rotation, layer boundary slip and particle–particle interactions, with  
408 minimal evidence of penetrative deformation, despite evidence from traditional strain markers such  
409 as reduction spots and deformed burrows (Meere et al., 2008). In these situations, using the  $R_f/\phi$   
410 methods leads to a significant underestimate of strain. More recently, Meere et al. (2016) highlighted  
411 the importance of identifying passive clast behaviour and the potential for deformation prior to  
412 lithification in understanding the deformation history of a region.

413

414 *Volume change*

415 Most studies applying the strain analysis techniques discussed, do not account for any potential  
416 volume change of the markers. Although Ramsay (1967) had already presented a modified Flinn  
417 diagram, which was capable of including some aspect of volume loss, this aspect of strain analysis is  
418 typically ignored. Clearly natural deformation rarely occurs in a closed system, and many attempts  
419 have been made at estimating volume reduction during deformation, as opposed to diagenetic  
420 volume loss. For example, there has been considerable debate regarding the amount of volume loss  
421 in slate belts. Sorby (1856) initially suggested that a 50% volume reduction could occur in slates, but  
422 settled on ~11% (1908). Wright and Platt (1982) suggested a volume loss of 50% in the Martinsburg  
423 Shale of West Virginia. Similar volume reductions were suggested in the Taconic Slate Belt (Goldstein  
424 et al., 1995, 1998). Onasch (1994) suggested a range of volume loss of 14-35% in deformed quartz  
425 arenites. Similarly, Markley and Wojtal (1996) suggested 10-15% volume loss in an Appalachian mixed  
426 siliciclastic sequence. Mosher (1987) analysed the variation in sizes of cobbles in the Purgatory  
427 Conglomerate, Rhode Island, and suggested that there could be a volume loss of 23-55% of the original  
428 cobble volumes in the areas of most intense deformation.

429 Despite these reports of significant volume reduction, these large volumes are rarely confirmed by  
430 geochemical analyses (Wintsch et al., 1991; Erslev and Ward, 1994; Tan et al., 1995). Similarly, Ramsay  
431 and Wood (1973) considered that a 10-20% volume reduction could occur based on density  
432 differences between lithified mudstones and slates, and argued that greater volume losses were likely  
433 to only occur in the deformation of incompletely consolidated sediments. As discussed earlier  
434 shortening values of this magnitude have been identified by in a range of settings (e.g., Cooper et al.,  
435 1983; Butler and Paton, 2010; Lathrop & Burberry, 2017).

436 While volume change has been mathematically incorporated into strain analysis (Gratier, 1983;  
437 Onasch and Davis, 1988; Baird and Hudleston, 2007), most rocks lack the necessary strain markers for  
438 this type of analysis. Some success has been made using isocon diagrams (Grant, 1986), but these are

439 typically restricted to discrete shear zones (Srivastava et al., 1995; Bhattacharyya and Hudleston,  
440 2001; Baird and Hudleston, 2007). Other successes in identifying volume loss has come from gravity  
441 driven fold and thrust belts, where the amount of extension high on the slope can be compared to the  
442 amount of compression towards the toe of the slope (Butler and Paton, 2010).

#### 443 **Conclusions**

444 Determining finite strain has seen significant developments since the seminal contribution of John  
445 Ramsay. Through advances in imaging and software, it is easier than ever before to collect large data  
446 sets and apply multiple strain analysis techniques rapidly, and there are a number of methods which  
447 can incorporate statistical handling of the results. Strain analysis is regularly incorporated into  
448 structural studies employing anisotropy of magnetic susceptibility, electron backscatter diffraction, x-  
449 ray tomography, microstructural analysis etc., which have not only led to advances in our knowledge  
450 of rock deformation processes, but also regional scale understanding. It should be obvious that  
451 detailed strain analysis studies are required to understand the spatial variations of strain in deformed  
452 terranes, but also the significance of those variations.

453 Of the many advances outlined here, most of them have been driven by developments in computing,  
454 automation and statistical methods, whilst the basis for these strain analysis techniques have by in  
455 large remained the same, which is a testament to the initial contribution of Ramsay. We anticipate  
456 that the next significant advances in this field will again be largely technologically driven. In particular,  
457 3D imaging of strain markers and 3D strain analysis should become more widespread, and perhaps  
458 developed into 4D. Although, there have been advances in applying micro-tomography to geological  
459 materials, these techniques are yet to be applied to strain analysis. There is also scope for advances  
460 to be made in the extraction of high quality data from images with minimum human intervention e.g.,  
461 grain boundary identification, and machine learning techniques could be applied to this. The natural  
462 optical heterogeneity of geological materials, even in single mineral phases such as quartz due to  
463 impurities, inclusions and microstructural features, will always makes the automation of grain

464 identification challenging. Increasingly the use of non-destructive chemical mapping techniques, for  
465 example using electron microscope energy-dispersive X-Ray spectroscopy (QEMSCAN) or Raman  
466 spectroscopy, produces outputs that allow the user to filter this heterogeneity thereby making the  
467 process of grain boundary identification more manageable. This, coupled with new machine learning  
468 techniques, will likely develop into a fully automated process for data acquisition, with strain analysis  
469 studies becoming fully automated and significantly more efficient.

470 Regardless of any future developments, it should be clear that the strain analysis techniques of  
471 Ramsay and their modernised equivalents should have a place in every structural geologist's toolbox.

472 **Acknowledgements**

473 We are grateful to Frederick Vollmer and Richard Lisle who both contributed critical and invaluable  
474 reviews that enhanced the text. Clare Bond is thanked for patient and helpful editorial assistance.  
475 Rachael Ellen is thanked for discussions that improved an earlier version of the manuscript. This paper  
476 is published with the permission of the Executive Director of the British Geological Survey (UKRI).

477 **References**

478 Adam, J., Klinkmueller, M., Schreurs, G., Wienke, B. 2013. Quantitative 3D strain analysis in analogue  
479 experiments simulating tectonic deformation: Integration of X-ray computed tomography and digital  
480 volume correlation techniques. *Journal of Structural Geology*, 55, 127-149.

481 Ailleres, L., Champenois, M., Macaudiere, J., Bertrand, J., 1995. Use of image analysis in the  
482 measurement of finite strain by the normalized Fry method: geological implications for the 'Zone  
483 Houillere' (Brianconnais zone, French Alps). *Mineralogical Magazine* 59, 179–187

484 Asmussen, P., Conrad, O., Günther, A., Kirsch, M. and Riller, U., 2015. Semi-automatic segmentation  
485 of petrographic thin section images using a “seeded-region growing algorithm” with an application to  
486 characterize weathered subarkose sandstone. *Computers & Geosciences*, 83, pp.89-99.

487 Baird, G.B. and Hudleston, P.J., 2007. Modeling the influence of tectonic extrusion and volume loss on  
488 the geometry, displacement, vorticity, and strain compatibility of ductile shear zones. *Journal of*  
489 *Structural Geology*, 29(10), pp.1665-1678.

490 Barraud, J., 2006. The use of watershed segmentation and GIS software for textural analysis of thin  
491 sections. *Journal of Volcanology and Geothermal Research*, 154(1-2), pp.17-33.

492 Bhattacharyya, P. and Hudleston, P., 2001. Strain in ductile shear zones in the Caledonides of northern  
493 Sweden: a three-dimensional puzzle. *Journal of Structural Geology*, 23(10), pp.1549-1565.

494 Borradaile, G.J., 1976. A strain study of a granite–granite gneiss transition and accompanying  
495 schistosity formation in the Betic orogenic zone, SE. Spain. *Journal of the Geological Society*, 132(4),  
496 pp.417-428.

497 Borradaile, G., 1987. Anisotropy of magnetic susceptibility: rock composition versus strain.  
498 *Tectonophysics*, 138(2-4), pp.327-329.

499 Borradaile, G.J. and Henry, B., 1997. Tectonic applications of magnetic susceptibility and its anisotropy.  
500 *Earth-Science Reviews*, 42(1-2), pp.49-93.

501 Borradaile, G.J. and Jackson, M., 2004. Anisotropy of magnetic susceptibility (AMS): magnetic  
502 petrofabrics of deformed rocks. *Geological Society, London, Special Publications*, 238(1), pp.299-360.

503 Boulter, C.A., 1976. Sedimentary fabrics and their relation to strain-analysis methods. *Geology*, 4(3),  
504 pp.141-146.

505 Brandon, M.T., 1995. Analysis of geologic strain data in strain-magnitude space. *Journal of Structural*  
506 *Geology*, 17(10), pp.1375-1385.

507 Breddin, H., 1954. Die tektonische Deformation der Fossilien im Rheinischen Schiefergebirge.  
508 *Zeitschrift der Deutschen Geologischen Gesellschaft*, pp.227-305.

509 Breddin, H., 1957. Tektonische Fossil-und Gesteinsdeformation im Gebiet von St. Goarshausen  
510 (Rheinisches Schiefergebirge): *Decheniana*, 110, pp.289-350.

511 Burberry, C.M., 2015. Spatial and temporal variation in penetrative strain during compression: Insights  
512 from analog models. *Lithosphere*, 7(6), pp.611-624.

513 Burmeister, K.C., Harrison, M.J., Marshak, S., Ferré, E.C., Bannister, R.A. and Kodama, K.P., 2009.  
514 Comparison of Fry strain ellipse and AMS ellipsoid trends to tectonic fabric trends in very low-strain  
515 sandstone of the Appalachian fold–thrust belt. *Journal of Structural Geology*, 31(9), pp.1028-1038.

516 Butler, R.W.H. and Paton, D.A., 2010. Evaluating lateral compaction in deepwater fold and thrust belts:  
517 How much are we missing from "nature's sandbox". *GSA Today*, 20(3), pp.4-10.

518 Cooper, M.A., Garton, M.R. and Hossack, J.R., 1983. The origin of the Basse Normandie duplex,  
519 Boulonnais, France. *Journal of Structural Geology*, 5(2), pp.139-152.

520 Cloos, E., 1947. Oölite deformation in the South Mountain fold, Maryland. *Geol. Soc. Am. Bull.* 58,  
521 843-918.

522 Choudhury, K.R., Meere, P.A. and Mulchrone, K.F., 2006. Automated grain boundary detection by  
523 CASRG. *Journal of Structural Geology*, 28(3), pp.363-375.

524 Crespi, J.M., 1986. Some guidelines for the practical application of Fry's method of strain analysis.  
525 *Journal of Structural Geology*, 8(7), pp.799-808.

526 Czeck, D.M., Fissler, D.A., Horsman, E. and Tikoff, B., 2009. Strain analysis and rheology contrasts in  
527 polymictic conglomerates: an example from the Seine metaconglomerates, Superior Province,  
528 Canada. *Journal of Structural Geology*, 31(11), pp.1365-1376.

529 De Paor, D.G., 1980. Some limitations of the  $R_f/\phi$  technique of strain analysis. *Tectonophysics*, 64(1-  
530 2), pp.T29-T31.

531 De Paor, D.G., 1988.  $R_f/\phi$  strain analysis using an orientation net. *Journal of Structural Geology*, 10(4),  
532 pp.323-333.

533 De Paor, D.G., 1990. Determination of the strain ellipsoid from sectional data. *Journal of Structural*  
534 *Geology*, 12(1), pp.131-137.

535 DeSitter, L., 1964. *Structural Geology*. Mc Graw-Hill.

536 DeVasto, Michael A., Dyanna M. Czeck, and Prajukti Bhattacharyya. "Using image analysis and ArcGIS®  
537 to improve automatic grain boundary detection and quantify geological images." *Computers &*  
538 *geosciences* 49 (2012): 38-45.

539 Dunne, W.M., Onasch, C.M. and Williams, R.T., 1990. The problem of strain-marker centers and the  
540 Fry method. *Journal of Structural Geology*, 12(7), pp.933-938.

541 Dunnet, D., 1969. A technique of finite strain analysis using elliptical particles. *Tectonophysics* 7, 117–  
542 136.

543 Dunnet, D., Siddans, A., 1971. Non-random sedimentary fabrics and their modification by strain.  
544 *Tectonophysics* 12, 307–325.

545 Elliott, D., 1970. Determination of finite strain and initial shape from deformed elliptical objects.  
546 *Geological Society of America Bulletin* 81, 2221–2236.

547 Erslev, E., 1988. Normalized center-to-center strain analysis of packed aggregates. *Journal of*  
548 *Structural Geology* 10, 201–209.

549 Erslev, E., Ge, H., 1990. Least-squares center-to-center and mean object ellipse fabric analysis. *Journal*  
550 *of Structural Geology* 12, 1047–1059.

551 Erslev, E. A., & Ward, D. J. (1994). Non-volatile element and volume flux in coalesced slaty cleavage.  
552 *Journal of Structural Geology*, 16(4), 531-553.

553 Flinn, D., 1956. On the deformation of the Funzie conglomerate, Fetlar, Shetland. *J. Geol.* 480–505.

554 Flinn, D., 1962a. On folding during three-dimensional progressive deformation. *Q. J. Geol. Soc.* 118.

555 Flinn, D., 1965. On the Symmetry Principle and the Deformation Ellipsoid. *Geol. Mag.* 102, 36–45.

556 Fossen, H., Tikoff, B. 1993. The deformation matrix for simultaneous simple shearing, pure shearing  
557 and volume change, and its applications to transpression-transension tectonics. *Journal of Structural*  
558 *Geology*, 15, 413-422.

559 Freeman, B., 1987. The behaviour of deformable ellipsoidal particles in three-dimensional slow flows:  
560 implications for geological strain analysis. *Tectonophysics*, 132(4), pp.297-309.

561 Freeman, B. and Lisle, R.J., 1987. The relationship between tectonic strain and the three-dimensional  
562 shape fabrics of pebbles in deformed conglomerates. *Journal of the Geological Society*, 144(4), pp.635-  
563 639.

564 Fry, N., 1979. Random point distributions and strain measurement in rocks. *Tectonophysics* 60, 89–  
565 105.

566 Gay, N.C. 1968a Pure shear and simple shear deformation of inhomogenous viscous fluids. 1. Theory.  
567 *Tectonophysics* 5, p 211-234.

568 Gay, N.C. 1968b Pure shear and simple shear deformation of inhomogenous viscous fluids. 2. The  
569 determination of total finite strain in a rock from objects such as deformed pebbles. *Tectonophysics*  
570 5, p 295-302.

571 Gay, N. C. 1969 The analysis of strain in the Barberton Mountain Land, Eastern Transvaal, using  
572 deformed pebbles. *Journal of Geology* 77, p 377-396.

573 Gendzwill, D.J. and Stauffer, M.R., 1981. Analysis of triaxial ellipsoids: Their shapes, plane sections,  
574 and plane projections. *Journal of the International Association for Mathematical Geology*, 13(2),  
575 pp.135-152.

576 Goldstein, A., Pickens, J., Klepeis, K. and Linn, F., 1995. Finite strain heterogeneity and volume loss in  
577 slates of the Taconic Allochthon, Vermont, USA. *Journal of Structural Geology*, 17(9), pp.1207-1216.

578 Goldstein, A., Knight, J. and Kimball, K., 1998. Deformed graptolites, finite strain and volume loss  
579 during cleavage formation in rocks of the taconic slate belt, New York and Vermont, USA. *Journal of*  
580 *structural geology*, 20(12), pp.1769-1782.

581 Goodchild, J.S. and Fueten, F., 1998. Edge detection in petrographic images using the rotating polarizer  
582 stage. *Computers & Geosciences*, 24(8), pp.745-751.

583 Gorsevski, P.V., Onasch, C.M., Farver, J.R. and Ye, X., 2012. Detecting grain boundaries in deformed  
584 rocks using a cellular automata approach. *Computers & Geosciences*, 42, pp.136-142.

585 Grant, J.A., 1986. The isocon diagram; a simple solution to Gresens' equation for metasomatic  
586 alteration. *Economic geology*, 81(8), pp.1976-1982.

587 Gratier, J.P., 1983. Estimation of volume changes by comparative chemical analyses in  
588 heterogeneously deformed rocks (folds with mass transfer). In *Strain Patterns in Rocks* (pp. 329-339).

589 Hanna, S., Fry, N., 1979. A comparison of methods of strain determination in rocks from southwest  
590 Dyfed (Pembrokeshire) and adjacent areas. *Journal of Structural Geology* 1, 155–162.

591 Houghton, S., 1856. LII. On slaty cleavage, and the distortion of fossils. London, Edinburgh, Dublin  
592 *Philos. Mag. J. Sci.* 12, 409–421.

593 Heilbronner, R., 2000. Automatic grain boundary detection and grain size analysis using polarization  
594 micrographs or orientation images. *Journal of Structural Geology* 22, 969–981.

595 Heilbronner, R. and Barrett, S., 2013. *Image analysis in earth sciences: microstructures and textures  
596 of earth materials* (Vol. 129). Springer Science & Business Media.

597 Hobbs, B.E. and Talbot, J.L., 1966. The analysis of strain in deformed rocks. *The Journal of Geology*,  
598 74(4), pp.500-513.

599 Hobbs, B.E., Means, W.D. and Williams, P.F., 1976. *An outline of structural geology*. Wiley.

600 Holst, T.B., 1982. The role of initial fabric on strain determination from deformed ellipsoidal objects.  
601 *Tectonophysics*, 82(3-4), pp.329

602 Hossack, J.R., 1968. Pebble deformation and thrusting in the Bygdin area (southern Norway).  
603 *Tectonophysics*, 5(4), pp.315-339.-350.

604 Hsu, T.C., 1966. The characteristics of coaxial and non-coaxial strain paths. *Journal of Strain Analysis*,  
605 1(3), pp.216-222.

606 Jungmann, M., Pape, H., Wißkirchen, P., Clauser, C. and Berlage, T., 2014. Segmentation of thin section  
607 images for grain size analysis using region competition and edge-weighted region merging. *Computers  
608 & Geosciences*, 72, pp.33-48.

609 Koyi, H.A., Sans, M., Teixell, A., Cotton, J. and Zeyen, H., 2004. The significance of penetrative strain in  
610 the restoration of shortened layers—Insights from sand models and the Spanish Pyrenees. In K. R.  
611 McClay, ed., *Thrust tectonics and hydrocarbon systems: AAPG Memoir 82*, p. 1–16.

612 Kumar, R., Srivastava, D.C. and Ojha, A.K., 2014. A comparison of the methods for objective strain  
613 estimation from the Fry plots. *Journal of Structural Geology*, 63, pp.76-90.

614 Lathrop, B.A. and Burberry, C.M., 2017. Accommodation of penetrative strain during deformation  
615 above a ductile décollement. *Lithosphere*, 9(1), pp.46-57.

616 Launeau, P., Bouchez, J.L. and Benn, K., 1990. Shape preferred orientation of object populations:  
617 automatic analysis of digitized images. *Tectonophysics*, 180(2-4), pp.201-211.

618 Launeau, P.A., and Robin, P.Y., 1996. Fabric analysis using the intercept method. *Tectonophysics*,  
619 267(1-4), pp.91-119.

620 Launeau, P. and Robin, P.Y.F., 2005. Determination of fabric and strain ellipsoids from measured  
621 sectional ellipses—Implementation and applications. *Journal of Structural Geology*, 27(12), pp.2223-  
622 2233.

623 Launeau, P., Archanjo, C.J., Picard, D., Arbaret, L. and Robin, P.Y., 2010. Two-and three-dimensional  
624 shape fabric analysis by the intercept method in grey levels. *Tectonophysics*, 492(1-4), pp.230-239.

625 Law, R.D., 1986. Relationships between strain and quartz crystallographic fabrics in the Roche Maurice  
626 quartzites of Plougastel, western Brittany. *Journal of Structural Geology*, 8(5), pp.493-515.

627 Leeder, M.R., 1982. *Sedimentology: process and product*. Springer.

628 Li, Y., Onasch, C.M. and Guo, Y., 2008. GIS-based detection of grain boundaries. *Journal of Structural*  
629 *Geology*, 30(4), pp.431-443.

630 Lisle, R., 1977a. Estimation of the tectonic strain ratio from the mean shape of deformed elliptical  
631 objects. *Geologie en Mijnbouw* 56, 140–144.

632 Lisle, R., 1977b. Clastic grain shape and orientation in relation to cleavage from the Aberystwyth Grits,  
633 Wales. *Tectonophysics* 39, 381–395.

634 Lisle, R.J., Rondeel, H.E., Doorn, D., Brugge, J. and Van de Gaag, P., 1983. Estimation of viscosity  
635 contrast and finite strain from deformed elliptical inclusions. *Journal of Structural Geology*, 5(6),  
636 pp.603-609.

637 Lisle, R., 1985. *Geological Strain Analysis: A Manual for the  $R_f/\phi$  Method*. Pergamon Press.

638 Lisle, R.J., 1985b. The effect of composition and strain on quartz-fabric intensity in pebbles from a  
639 deformed conglomerate. *Geologische Rundschau*, 74(3), pp.657-663.

640 Lisle, R., 1994. Palaeostrain Analysis. In P.L. Hancock (Ed.), *Continental Deformation*, Pergamon Press,  
641 pp. 28-42.

642 Lisle, R.J., 2010. Strain analysis from point fabric patterns: An objective variant of the Fry method.  
643 *Journal of Structural Geology*, 32(7), pp.975-981.

644 Louis, L., Wong, T., Buad, P. Tembe, S. 2006. Imaging strain localization by X-ray computed  
645 tomography: discrete compaction bands in Diemelstadt sandstone. *Journal of Structural Geology*, 28,  
646 762-775.

647 Maffione, M. and Morris, A., 2017. The onset of fabric development in deep marine sediments. *Earth*  
648 *and Planetary Science Letters*, 474, pp.32-39.

649 Mandal, N., Samanta, S.K., Bhattacharyya, G. and Chakraborty, C., 2003. Deformation of ductile  
650 inclusions in a multiple inclusion system in pure shear. *Journal of Structural Geology*, 25(9), pp.1359-  
651 1370.

652 Marjoribanks, R.W., 1976. The relation between microfabric and strain in a progressively deformed  
653 quartzite sequence from central Australia. *Tectonophysics*, 32(3-4), pp.269-293.

654 Markley, M. and Wojtal, S., 1996. Mesoscopic structure, strain, and volume loss in folded cover strata,  
655 Valley and Ridge Province, Maryland. *American Journal of Science*, 296(1), pp.23-57.

656 Masuda, T., Koike, T., Yuko, T. and Morikawa, T., 1991. Discontinuous grain growth of quartz in  
657 metacherts: the influence of mica on a microstructural transition. *Journal of Metamorphic Geology*,  
658 9(4), pp.389-402.

659 Matthews, P.E., Bond, R.A.B. and Van Den Berg, J.J., 1974. An algebraic method of strain analysis using  
660 elliptical markers. *Tectonophysics*, 24(1-2), pp.31-67.

661 McCarthy, D.J., Meere, P.A. and Petronis, M.S., 2015. A comparison of the effectiveness of clast based  
662 finite strain analysis techniques to AMS in sandstones from the Sevier Thrust Belt, Wyoming.  
663 *Tectonophysics*, 639, pp.68-81.

664 McNaught, M, 1994. Modifying the normalized Fry method for aggregates of non-elliptical grains.  
665 *Journal of Structural Geology*, 16(4), pp.493-503.

666 Means, W.D., Hobbs, B.E., Lister, G.S., Williams, P.F. 1980. Vorticity and non-coaxiality in progressive  
667 deformation. *Journal of Structural Geology*, 2, 371-378.

668 Meere, P.A., Mulchrone, K.F., Sears, J.W. and Bradway, M.D., 2008. The effect of non-passive clast  
669 behaviour in the estimation of finite strain in sedimentary rocks. *Journal of Structural Geology*, 30(10),  
670 pp.1264-1271.

671 Meere, P.A., Mulchrone, K.F., McCarthy, D.J., Timmerman, M.J. and Dewey, J.F., 2016. Prelithification  
672 and synlithification tectonic foliation development in a clastic sedimentary sequence. *Geology*, 44(4),  
673 pp.291-294.

674 Miller, D.M. and Christie, J.M., 1981. Comparison of quartz microfabric with strain in recrystallized  
675 quartzite. *Journal of Structural Geology*, 3(2), pp.129-141.

676 Milton, N.J., 1980. Determination of the strain ellipsoid from measurements on any three sections.  
677 *Tectonophysics*, 64(1-2), pp.T19-T27.

678 Mingireanov Filho, I., Spina, T.V., Falcão, A.X. and Vidal, A.C., 2013. Segmentation of sandstone thin  
679 section images with separation of touching grains using optimum path forest operators. *Computers &*  
680 *Geosciences*, 57, pp.146-157.

681 Mitra, G., 1994. Strain variation in thrust sheets across the Sevier fold-and-thrust belt (Idaho-Utah-  
682 Wyoming): Implications for section restoration and wedge taper evolution. *Journal of Structural*  
683 *Geology*, 16(4), pp.585-602.

684 Mookerjee, M., Nickleach, S., 2011. Three-dimensional strain analysis using Mathematica. *J. Struct.*  
685 *Geol.* 33, 1467–1476.

686 Mookerjee, M. and Peek, S., 2014. Evaluating the effectiveness of Flinn's k-value versus Lode's ratio.  
687 *Journal of Structural Geology*, 68, pp.33-43.

688 Mosher, S., 1987. Pressure-solution deformation of the Purgatory Conglomerate, Rhode Island (USA):  
689 quantification of volume change, real strains and sedimentary shape factor. *Journal of structural*  
690 *geology*, 9(2), pp.221-232.

691 Mukul, M., 1998. A spatial statistics approach to the quantification of finite strain variation in  
692 penetratively deformed thrust sheets: an example from the Sheeprock Thrust Sheet, Sevier. *Journal*  
693 *of Structural Geology* 20, 371–384.

694 Mulchrone, K.F. and Meere, P.A., 2001. A Windows program for the analysis of tectonic strain using  
695 deformed elliptical markers. *Computers & geosciences*, 27(10), pp.1251-1255.

696 Mulchrone, K.F., 2003. Application of Delaunay triangulation to the nearest neighbour method of  
697 strain analysis. *Journal of Structural Geology*, 25(5), pp.689-702.

698 Mulchrone, K.F., O'Sullivan, F. and Meere, P.A., 2003. Finite strain estimation using the mean radial  
699 length of elliptical objects with bootstrap confidence intervals. *Journal of Structural Geology*, 25(4),  
700 pp.529-539.

701 Mulchrone, K.F., Meere, P.A. and Choudhury, K.R., 2005. SAPE: a program for semi-automatic  
702 parameter extraction for strain analysis. *Journal of structural geology*, 27(11), pp.2084-2098.

703 Mulchrone, K.F. and Walsh, K., 2006. The motion of a non-rigid ellipse in a general 2D deformation.  
704 *Journal of Structural Geology*, 28(3), pp.392-407.

705 Mulchrone, K.F., 2013. Fitting the void: Data boundaries, point distributions and strain analysis.  
706 *Journal of Structural Geology*, 46, pp.22-33.

707 Mulchrone, K.F., McCarthy, D.J. and Meere, P.A., 2013. Mathematica code for image analysis, semi-  
708 automatic parameter extraction and strain analysis. *Computers & Geosciences*, 61, pp.64-70.

709 Nádai, A., 1950. *Theory of flow and fracture of solids*, v. 2.

710 Oertel, G., 1978. Strain determination from the measurement of pebble shapes. *Tectonophysics*,  
711 50(1), pp.T1-T7.

712 Onasch, C.M., 1986. Ability of the Fry method to characterize pressure-solution deformation.  
713 *Tectonophysics*, 122(1-2), pp.187-193.

714 Onasch, C.M., 1994. Assessing brittle volume-gain and pressure solution volume-loss processes in  
715 quartz arenite. *Journal of Structural Geology*, 16(4), pp.519-530.

716 Onasch, C.M. and Davis, T.L., 1988. Strain determination using cathodoluminescence of calcite  
717 overgrowths. *Journal of structural geology*, 10(3), pp.301-303.

718 Owens, W.H., 1984. The calculation of a best-fit ellipsoid from elliptical sections on arbitrarily  
719 orientated planes. *J. Struct. Geol.* 6, 571–578.

720 Panozzo, R., 1984. Two-dimensional strain from the orientation of lines in a plane. *Journal of Structural*  
721 *Geology* 6, 215–221.

722 Panozzo, R., 1987. Two-dimensional strain determination by the inverse SURFOR wheel. *Journal of*  
723 *Structural Geology*, 9(1), pp.115-119.

724 Park, R.G., 1997. *Foundation of structural geology*. Routledge.

725 Passchier, C.W. and Trouw, R.A., 2005. *Microtectonics (Vol. 1)*. Springer Science & Business Media.

726 Paterson, S., Yu, H., 1994. Primary fabric ellipsoids in sandstones: implications for depositional  
727 processes and strain analysis. *J. Struct. Geol.* 16, 505–517.

728 Peach, C., and Lisle, R., 1979. A Fortran IV program for the analysis of tectonic strain using deformed  
729 elliptical markers. *Computers & Geosciences* 5, 325–334.

730 Perring, C.S., Barnes, S.J., Verrall, M. and Hill, R.E.T., 2004. Using automated digital image analysis to  
731 provide quantitative petrographic data on olivine–phyric basalts. *Computers & Geosciences*, 30(2),  
732 pp.183-195.

733 Phillips, J., 1843. On certain movements in the parts of stratified rocks. *Adv. Sci*, pp.60-61.

734 Prior, D.J., Mariani, E. and Wheeler, J., 2009. EBSD in the earth sciences: applications, common  
735 practice, and challenges. In *Electron backscatter diffraction in materials science* (pp. 345-360).  
736 Springer, Boston, MA.

737 Protzman, G.M. and Mitra, G., 1990. Strain fabric associated with the Meade thrust sheet: implications  
738 for cross-section balancing. *Journal of Structural Geology*, 12(4), pp.403-417.

739 Ramsay, J.G., 1967. Folding and fracturing of rocks. New York, MacGraw-Hill, 568p

740 Ramsay, J.G. and Wood, D.S., 1973. The geometric effects of volume change during deformation  
741 processes. *Tectonophysics*, 16(3-4), pp.263-277.

742 Ramsay, J.G., and Huber, M., 1983. The techniques of modern structural geology. *Strain Analysis*,  
743 London: Academic Press.

744 Reddy, B.S.R. and Srivastava, D.C., 2012. Rapid extraction of central vacancy by image-analysis of Fry  
745 plots. *Journal of Structural Geology*, 40, pp.44-53.

746 Robin, P., 1977. Determination of geologic strain using randomly oriented strain markers of any shape.  
747 *Tectonophysics* 42, T7–T16.

748 Robin, P.-Y.F., 2002. Determination of fabric and strain ellipsoids from measured sectional ellipses —  
749 theory. *J. Struct. Geol.* 24, 531–544.

750 Robin P.F., Charles, C.R.J. 2015. Quantifying the three-dimensional shapes of spheroidal objects in  
751 rocks imaged by tomography. *Journal of Structural Geology*, 77, 1-10.

752 Seymour, D.B. and Boulter, C.A., 1979. Tests of computerised strain analysis methods by the analysis  
753 of simulated deformation of natural unstrained sedimentary fabrics. *Tectonophysics*, 58(3-4), pp.221-  
754 235.

755 Shan, Y., 2008. An analytical approach for determining strain ellipsoids from measurements on planar  
756 surfaces. *Journal of Structural Geology*, 30(4), pp.539-546

757 Shan, Y. and Xiao, W., 2011. A statistical examination of the Fry method of strain analysis. *Journal of*  
758 *Structural Geology*, 33(5), pp.1000-1009.

759 Shao, J. and Wang, C., 1984. Determination of strain ellipsoid according to two-dimensional data on  
760 three or more intersection planes. *Journal of the International Association for Mathematical Geology*,  
761 16(8), pp.823-833.

762 Sharpe, D., 1847. On slaty cleavage. *Q. J. Geol. Soc.* 3, 74–105.

763 Shimamoto, T., Ikeda, Y., 1976. A simple algebraic method for strain estimation from deformed  
764 ellipsoidal objects. 1. Basic theory. *Tectonophysics* 36, 315–337.

765 Siddans, A.W.B., 1980. Analysis of three-dimensional, homogeneous, finite strain using ellipsoidal  
766 objects. *Tectonophysics*, 64(1-2), pp.1-16.

767 Soares, A. and Dias, R., 2015. Fry and  $R_f/\phi$  strain methods constraints and fold transection  
768 mechanisms in the NW Iberian Variscides. *Journal of Structural Geology*, 79, pp.19-30.

769 Sorby, H., 1849. On the origin of slaty cleavage. *Proc. Geol. Polytech. Soc. West Rid. Yorksh.* 3, 300–  
770 312.

771 Sorby, H., 1856. XVIII. On the theory of the origin of slaty cleavage. London, Edinburgh, Dublin *Philos.*  
772 *Mag. J. Sci.* 12, 127–129.

773 Sorby, H.C., 1908. On the application of quantitative methods to the study of the structure and history  
774 of rocks. *Quarterly Journal of the Geological Society*, 64(1-4), pp.171-233.

775 Srivastava, H.B., Hudleston, P. and Earley III, D., 1995. Strain and possible volume loss in a high-grade  
776 ductile shear zone. *Journal of Structural Geology*, 17(9), pp.1217-1231.

777 Tan, B.K., Gray, D.R. and Stewart, I., 1995. Volume change accompanying cleavage development in  
778 graptolitic shales from Gisborne, Victoria, Australia. *Journal of Structural Geology*, 17(10), pp.1387-  
779 1394.

780 Tarquini, S. and Favalli, M., 2010. A microscopic information system (MIS) for petrographic analysis.  
781 *Computers & Geosciences*, 36(5), pp.665-674.

782 Tikoff, B, Fossen, H. 1993. Simultaneous pure and simple shear: the unifying deformation matrix.  
783 *Tectonophysics*, 217, 267-283.

784 Tikoff, B, Fossen, H. 1995. The limitations of three dimensional kinematic vorticity analysis. Journal of  
785 Structural Geology, 17, 1771-1784.

786 Tikoff, B, Fossen, H. 1999. Three dimensional reference deformations and strain facies. Journal of  
787 Structural Geology, 21, 1497-1512. Todd, S.P., 2000, Taking the roof off a suture zone: basin setting  
788 and provenance of conglomerates in the ORSDingle Basin of SW Ireland: Geological Society, London,  
789 Special Publications, v. 180, no. 1, p. 185–222.

790 Treagus, S.H., 2002. Modelling the bulk viscosity of two-phase mixtures in terms of clast shape. Journal  
791 of Structural Geology, 24(1), pp.57-76.

792 Treagus, S.H., and Treagus, J.E., 2002. Studies of strain and rheology of conglomerates. J. Struct. Geol.  
793 24, 1541–1567.

794 Van den Berg, E.H., Meesters, A.G.C.A., Kenter, J.A.M. and Schlager, W., 2002. Automated separation  
795 of touching grains in digital images of thin sections. Computers & Geosciences, 28(2), pp.179-190.

796 Vitale, S. and Mazzoli, S., 2005. Influence of object concentration on finite strain and effective viscosity  
797 contrast: insights from naturally deformed packstones. Journal of Structural Geology, 27(12), pp.2135-  
798 2149.

799 Vollmer, F. W., 2010. A comparison of ellipse-fitting techniques for two and three-dimensional strain  
800 analysis, and their implementation in an integrated computer program designed for field-based  
801 studies. Abstract T21B-2166, Fall Meeting, American Geophysical Union, San Francisco, California.

802 Vollmer, F. W., 2011. Best-fit strain from multiple angles of shear and implementation in a computer  
803 program for geological strain analysis. Geological Society of America Abstracts with Programs, v. 43.

804 Vollmer, F. W., 2017. EllipseFit: Strain and Fabric Analysis Software User Manual Version 3.4.0  
805 [computer software user manual]. Retrieved from <http://www.frederickvollmer.com/ellipsefit/>.

806 Waldron, J.W. and Wallace, K.D., 2007. Objective fitting of ellipses in the centre-to-centre (Fry)  
807 method of strain analysis. *Journal of Structural Geology*, 29(9), pp.1430-1444.

808 Weil, A.B. and Yonkee, A., 2009. Anisotropy of magnetic susceptibility in weakly deformed red beds  
809 from the Wyoming salient, Sevier thrust belt: Relations to layer-parallel shortening and orogenic  
810 curvature. *Lithosphere*, 1(4), pp.235-256.

811 Wheeler, J., 1986. Strain analysis in rocks with pre-tectonic fabrics. *Journal of structural geology*, 8(8),  
812 pp.887-896.

813 Wintsch, R.P., Kvale, C.M. and Kisch, H.J., 1991. Open-system, constant-volume development of slaty  
814 cleavage, and strain-induced replacement reactions in the Martinsburg Formation, Lehigh Gap,  
815 Pennsylvania. *Geological Society of America Bulletin*, 103(7), pp.916-927.

816 Woodward, N.B., Gray, D.R. and Spears, D.B., 1986. Including strain data in balanced cross-sections.  
817 *Journal of Structural Geology*, 8(3-4), pp.313-324.

818 Wright, T.O. and Platt, L.B., 1982. Pressure dissolution and cleavage in the Martinsburg Shale.  
819 *American Journal of Science*, 282(2), pp.122-135.

820 Yu, H., Zheng, Y., 1984. A statistical analysis applied to the  $R_f/\phi$  method. *Tectonophysics* 110, 151–  
821 155.

822 Zingg, T., 1935. Beitrag zur schotteranalyse (Doctoral dissertation, ETH Zurich).

823

824

825 **Figure Captions**

826 Fig. 1 Identifying strain in rocks. A. A highly idealised rock outcrop with three exposed mutually  
827 perpendicular surfaces, with appropriate strain markers on each surface. The strain ellipsoid illustrates  
828 the relationship between the tectonic stretching axes XYZ and sigma 1, 2 & 3. B. A real outcrop from  
829 the Dingle Peninsula, which presents a more challenging problem for identifying and quantifying  
830 strain.

831 Fig. 2 A. Measuring the long (M) and short (m) axes of elliptical strain markers. B. Plot of the long and  
832 short axes from A. The slope of a best-fit line that passes through the points and the origin provides  
833 an estimate of the strain ratio. C. Measuring chords along three defined directions for a population of  
834 ellipses.

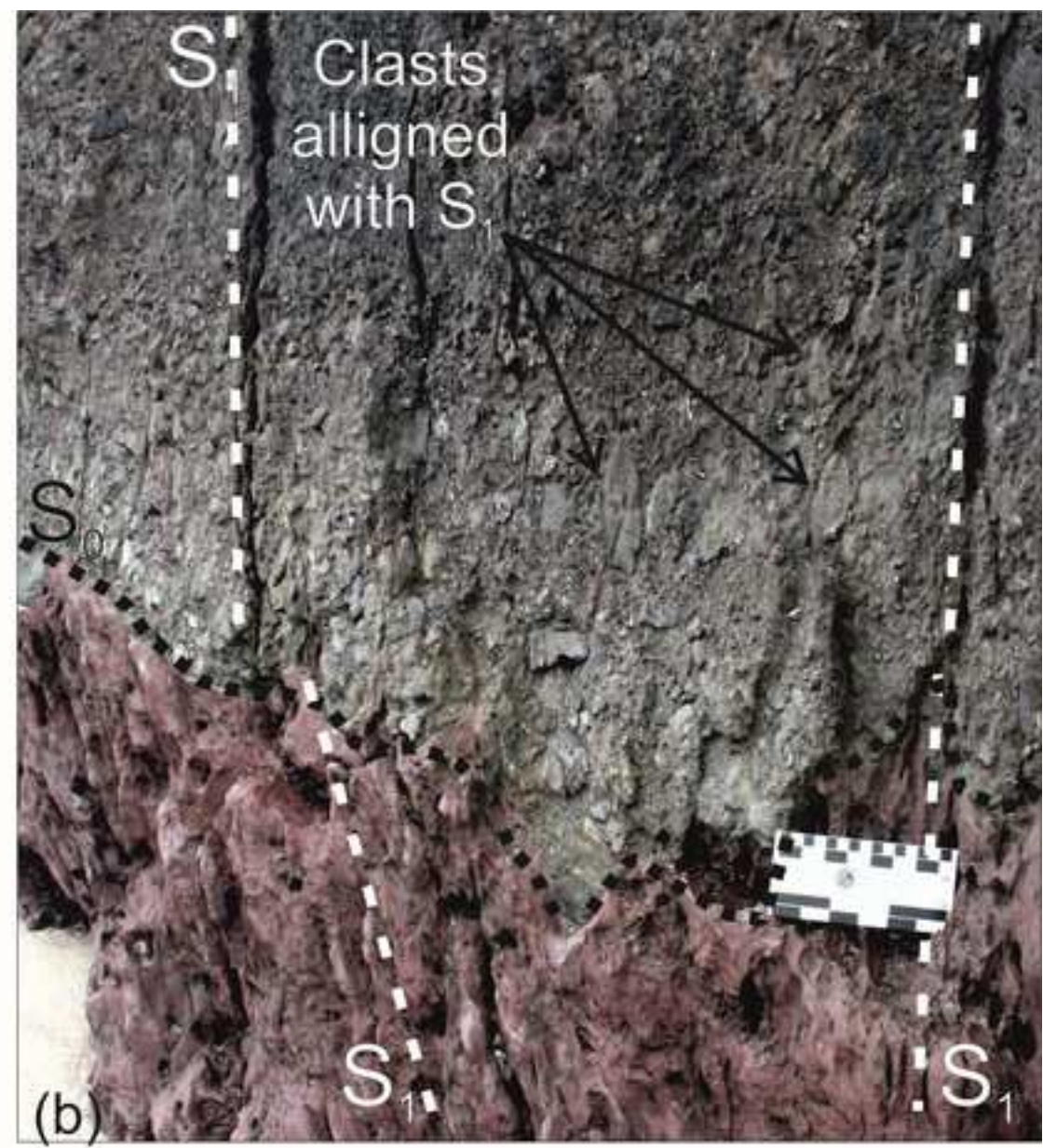
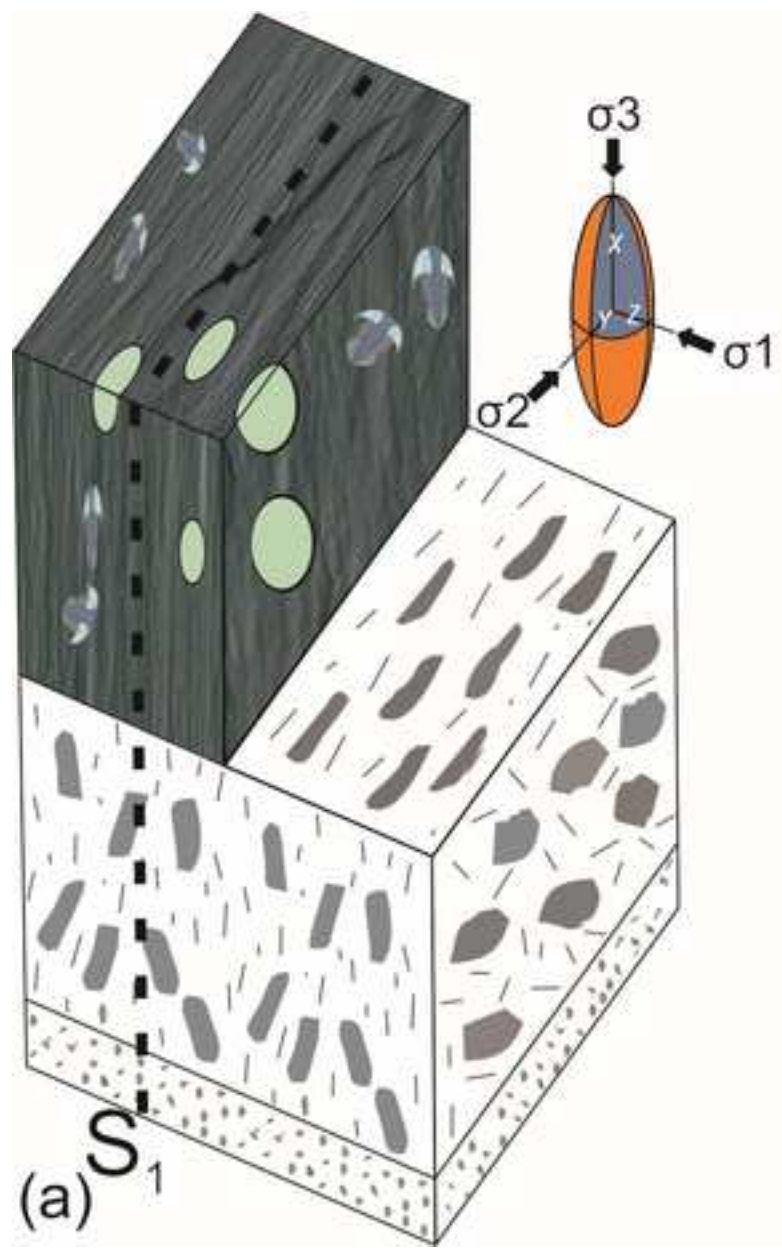
835 Fig. 3 Nearest-neighbour and or centre-to-centre methodology. A. Centre to centre techniques are  
836 based on the assumption that the tie-lines between nearest neighbours have a uniformly random  
837 distribution in the unstrained state. The lengths, d, and orientations,  $\alpha$ , of tie lines joining object  
838 centres are marked. The Polar plot of the unstrained state is illustrated below, showing d vs  $\alpha$ .  
839 Interestingly, this unstrained sample has a weak preferred distribution, in that the clasts are closer  
840 together in the vertical direction than the horizontal direction. B. Initial strained state, the distances  
841 between clasts become shorter in the tectonic shortening direction. The polar plot indicates higher  
842 strain estimates. The apex of the curve shows the orientation of the longest direction and the nadir  
843 shows the orientation of the shortest direction. C. The final strain state with pressure solution and a  
844 higher strain estimate.

845 Fig. 4 The  $R_f/\phi$  method. A. After fitting ellipses to strain markers, the ratio of the long axis to short  
846 axis is calculated and the orientation relative to a reference angle is recorded. B. These ratios are then  
847 plotted against the orientation of the long axis. This limited data set suggests that preferred  
848 orientation is between 45 degrees and 75 degrees. Clearly more data is required to more accurately  
849 estimate strain.

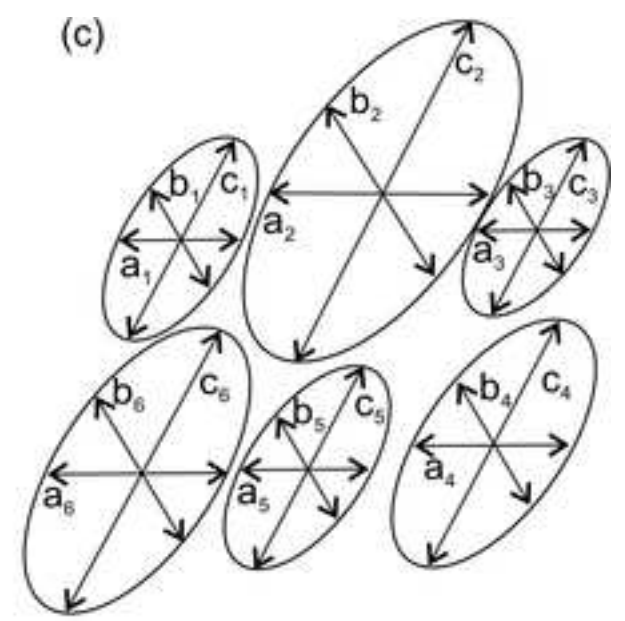
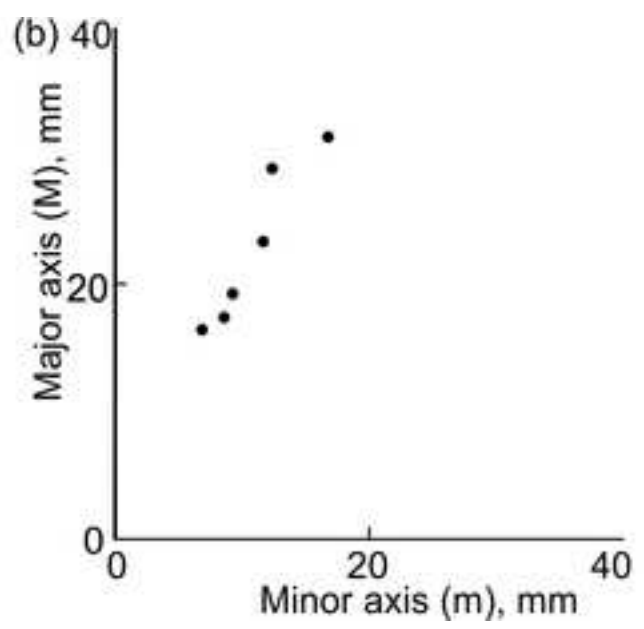
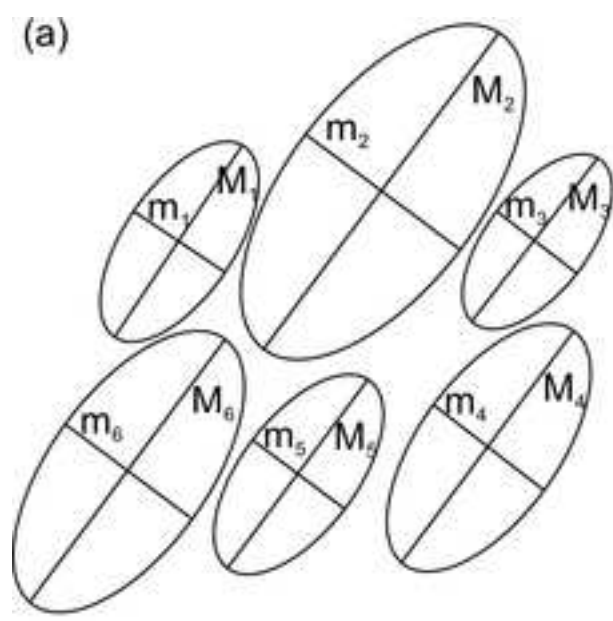
850 Fig. 5. Flinn and Nadai-Hsu plots. A. Flinn plots represent all possible ellipsoid geometries in a 2D space.  
851 The standard convention is to use a logarithmic plot, where the ratio of the maximum to intermediate  
852 ellipsoid axes ( $\ln X/Y$ ) is plotted as ordinate and the ratio of the minimum to intermediate axes ( $\ln$   
853  $Y/Z$ ) is plotted as abscissa. Prolate spheroids plot along the vertical axis and oblate spheroids plot along  
854 the horizontal. As these ellipsoids become less spherical, they plot further away from the origin. B.  
855 Nadai-Hsu plots show similar information to the Flinn Plots, but have an advantage that less deformed  
856 ellipsoids plot closer together regardless of shape.

857 Fig. 6. Typical strain analysis methodology. A. Selection of a suitable oriented thin section. B. Fitting  
858 ellipses to the clasts shown in A. C. Fitting the central void of the Fry Plot. D. The same data is  
859 presented in a polar plot. E. Strain estimate from the DTNNM method represented by the black star.  
860 The shaded ellipses represent the Bootstrapped confidence intervals. F. Strain estimate from the MRL  
861 method represented by the black star. The shaded ellipses represent the Bootstrapped confidence  
862 intervals. Note the underestimate compared to the DTNNM method.

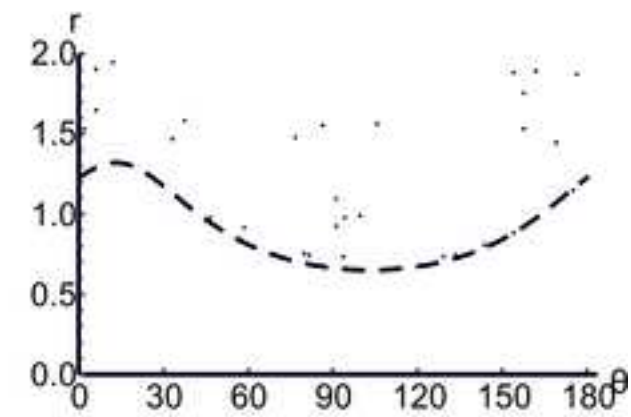
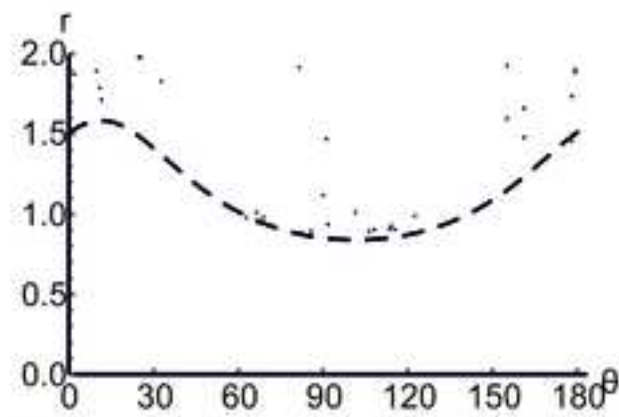
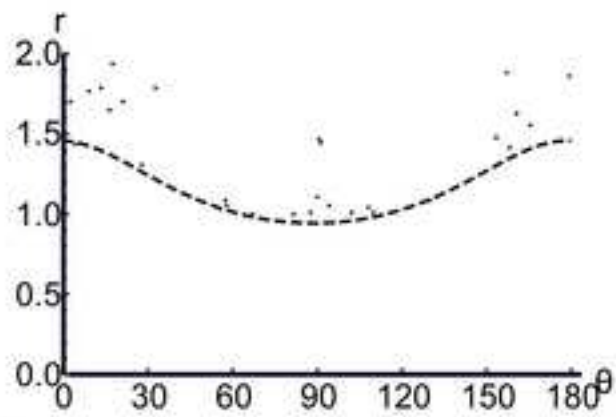
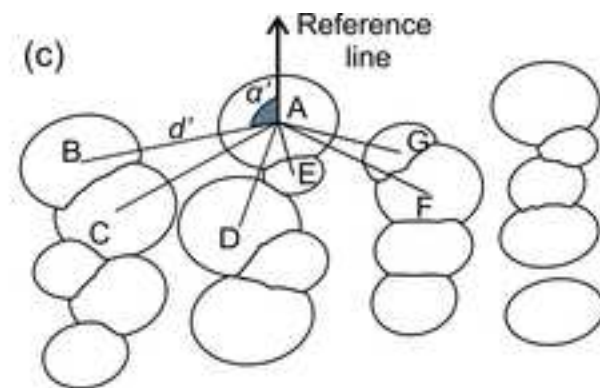
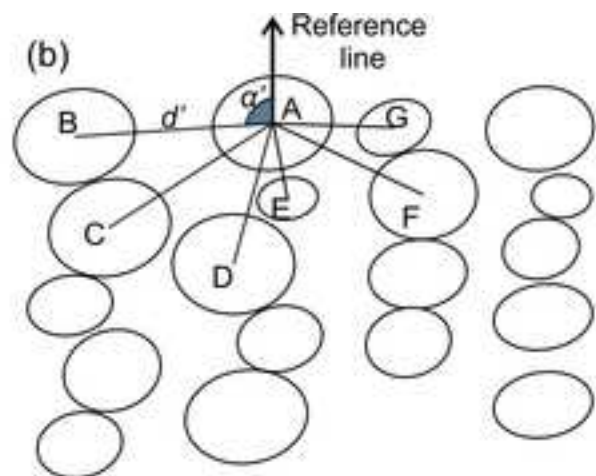
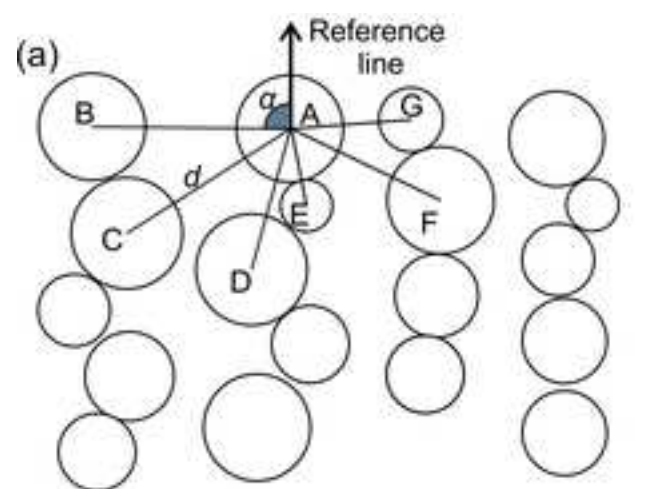
Figure



Figure



Figure

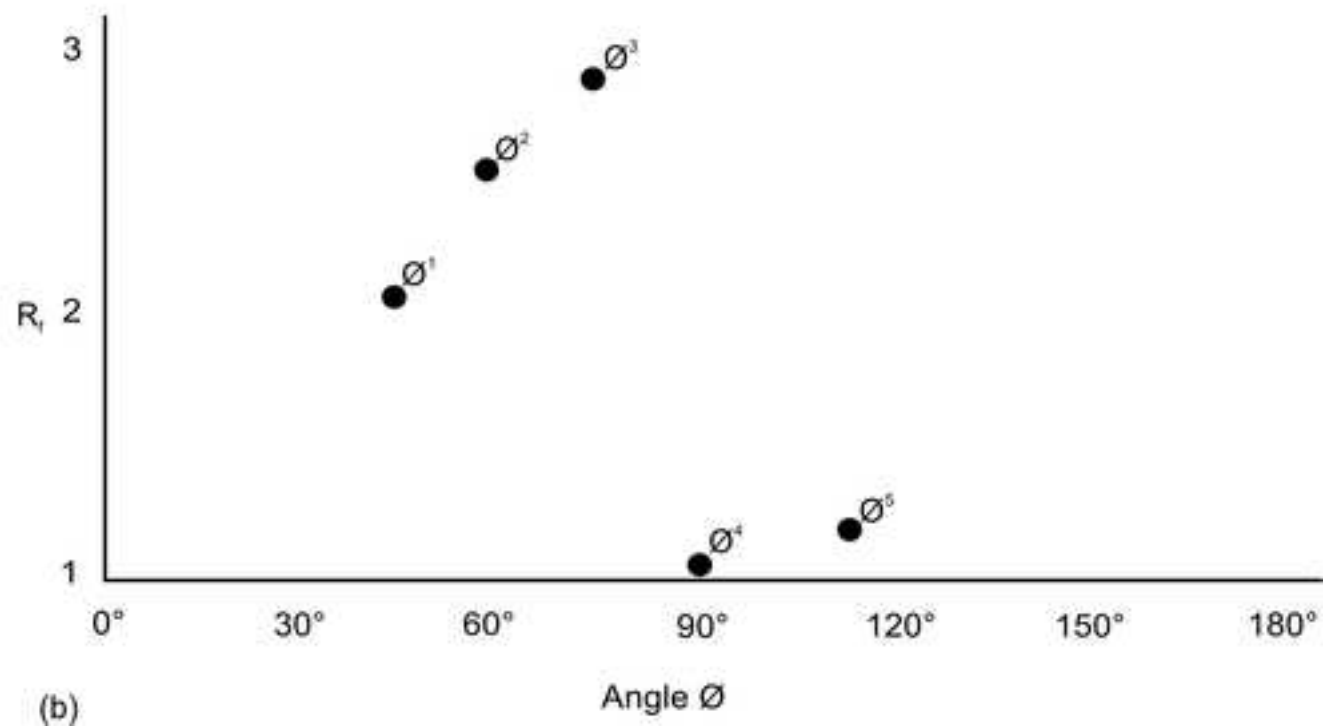
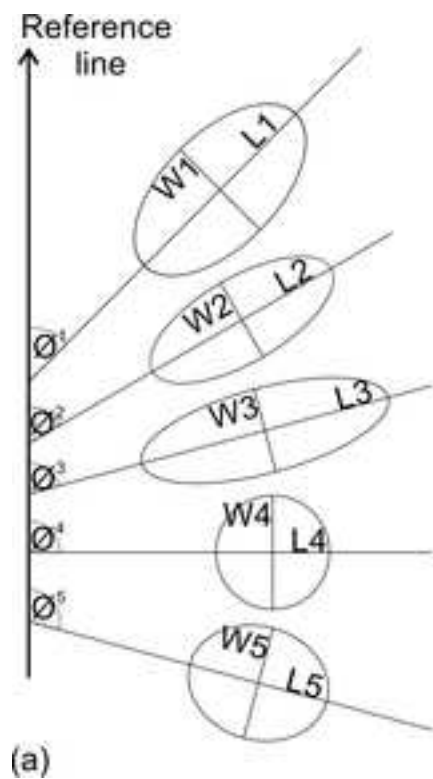


(d)

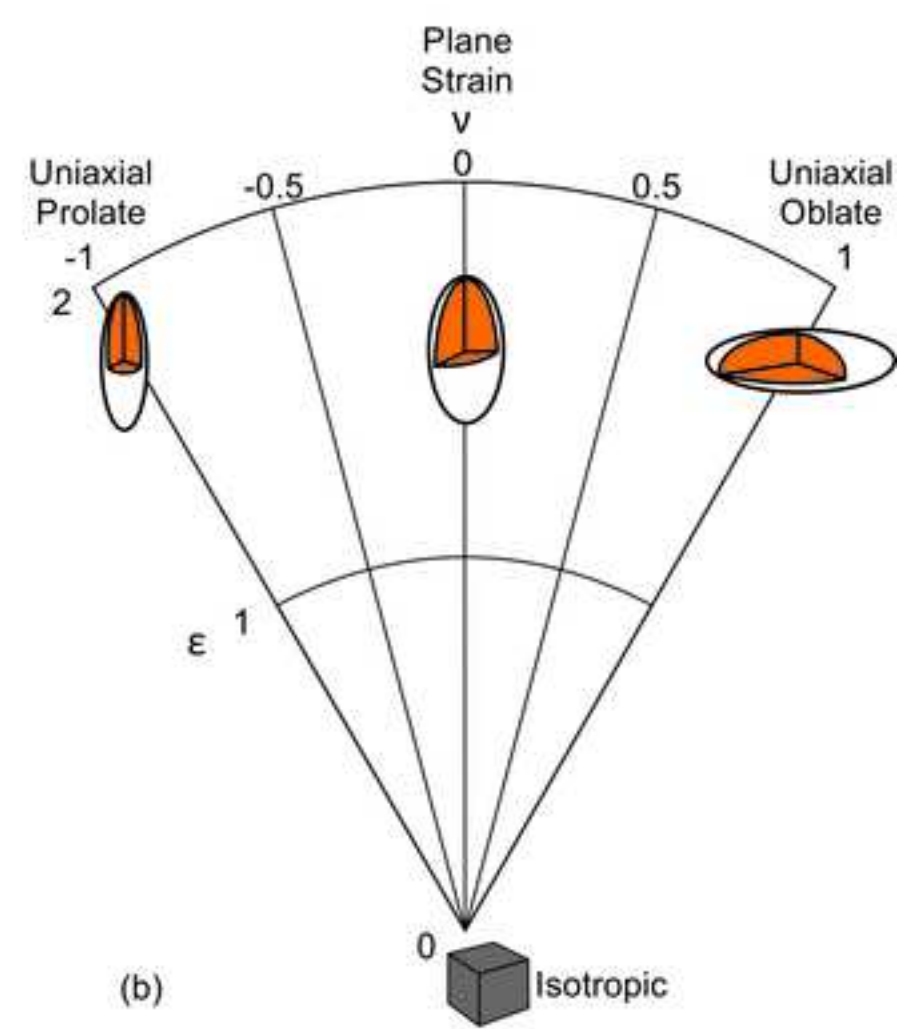
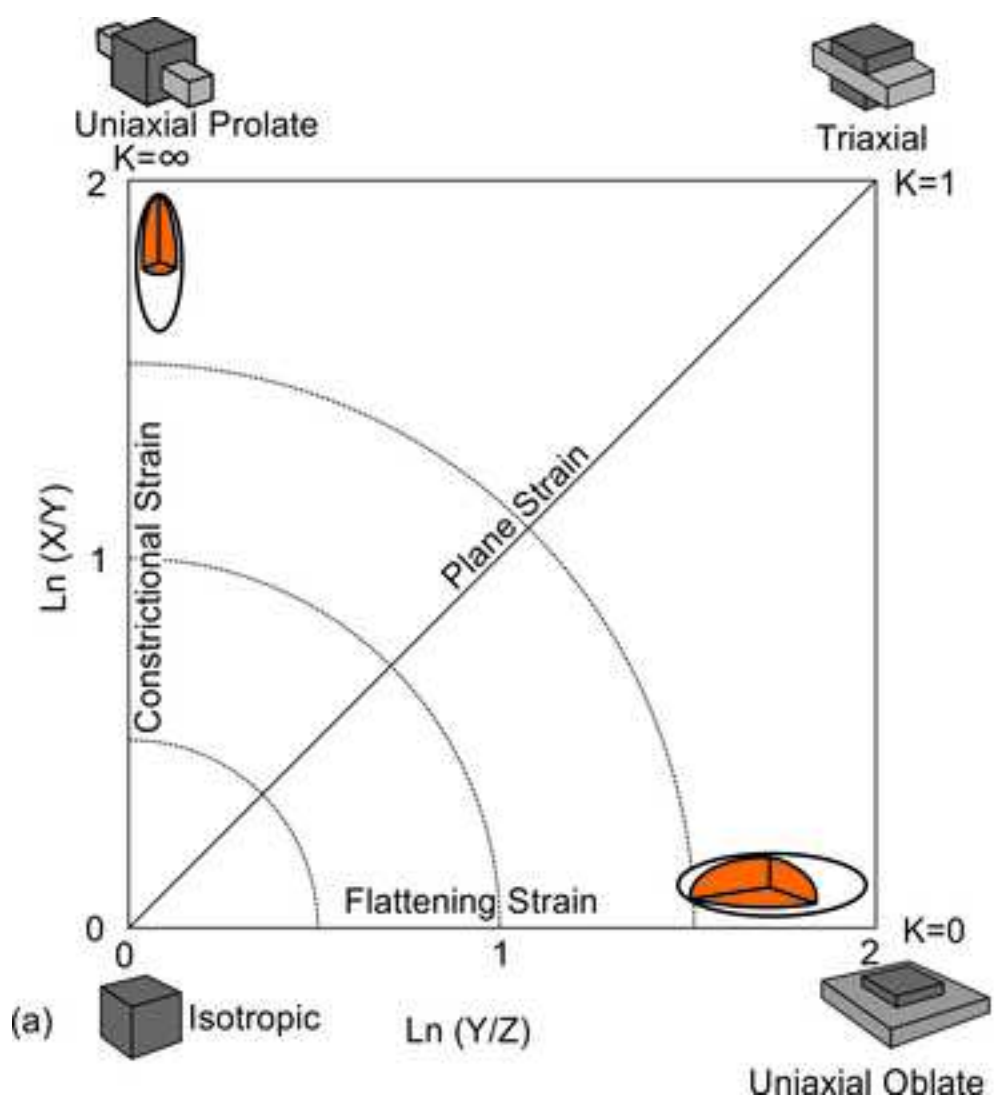
(e)

(f)

Figure



Figure



Figure

